

J. C. R. Hunt^{1,3}, A. Orr¹, D. Cresswell¹ & A. Owinoh²

(1) Centre for Polar Observation & Modelling, University College London

(2) Potsdam Institute for Climate Impact Research

(3) also TU Delft

A general linearised ‘shallow-layer’ perturbation model, where the approximately neutral lower layer of thickness h_o is situated below a stable upper layer or inversion layer, is developed for idealised and steady, but typical, mesoscale atmospheric flows. Significant Coriolis effects and variations in surface conditions (surface roughness, mountainous elevation, thermal effects on slopes) are considered. The model equations are solved here when the Froude number of the lower layer is small and where the surface drag roughness and surface elevation are modelled as a distributed body force through the lower layer. The results are compared with linear continuously stratified idealised model [10] and non-linear model (UK Unified Model) computations for particular flows over the mountains of Greenland and the coast of the Kent Peninsula/northern France. It is demonstrated that the simpler shallow layer model leads to some useful general concepts and quantitative estimates for a wide range of perturbed mesoscale flows, especially where the surface conditions change sharply over scales of order 1-10km. The main results of meteorological interest are that: (i) The upwind extent of the flow perturbation is of order of the Rossby deformation radius L_R , but that if the stratification is constant with height this distance is of order of the width B of the surface condition change (if $B > L_R$). For most significant mountain chains the former is the relevant distance. (ii) If the wind direction is parallel to the edge-line separating the change in surface drag roughness or change in elevation, there are marked positive and negative perturbations in the mean velocity across the edge-line over a horizontal distance of order h_o , explaining very high coastal winds within 1km of the coast. The effects of surface drag, but not the elevation, increase the windspeed perturbation in the downwind direction until limited by non-linear effects. These positive and negative wind ‘jets’, which do not occur in the absence of Coriolis effects, decrease away from the edge-line gradually over transverse length scales of order L_R . (iii) In flows approaching parallel to, or at an angle to, the edge-line, the height h_o varies, for example, increasing inland over a distance L_R when stable airflow approaches from the sea. This explains the observed increasing cloudiness inland from the coast. (iv) Features of the shallow layer flow are consistent with present and previous numerical mesoscale results when the grid scale is of order h_o or less (i.e. 2km). Certain broad features, e.g. wind jets in the wake of mountains, are well captured even at coarser resolutions of 12km. (v) The analysis provides a method of estimating errors associated with finite grid size in numerical mesoscale models. The same methods and concepts apply to hydraulic flows and stratified ocean flows below ice bergs etc and above any undulating bottom.

1 INTRODUCTION

Some of the changes that occur in mesoscale atmospheric flows (defined here as scales less than 100km) are driven by gradients of surface conditions, such as surface roughness, elevation, and temperature or heat flux. As an example of how difficult these flows can be to predict, the flow over and around Greenland is affected by the large elevation change between the coastal margins and the central plateau (~ 3 km), the combination of very rough surfaces and jagged mountains around the coasts, and the strong katabatic flows

from the plateau down to the coasts [13] [7]. The extremely sharp gradients in roughness and elevation result in local scale phenomena (e.g. coastal wind-jets) that have long been observed but are only described by mesoscale models when they are run with fine resolution (e.g. [10] [3]). But these local scale phenomena can have large scale climate effects, e.g. drag, wind waves, upwelling, etc.

Recent computations (e.g. [6] [3]) have shown how mesoscale flows can be strongly affected by stable stratification and Coriolis acceleration caused by

changes in surface roughness and the drag of mountains. Earlier studies showed how inviscid and viscous stratified rotating flow is affected by the effects of changes in elevation (e.g. [2] [15]). But there have been no general estimates about the relative magnitudes of these effects and consequences for local wind fields over the natural length scale of these flows, the Rossby deformation radius $L_R = Nh_o/f$ (based on inversion layer height h_o or alternatively the mountain height H , buoyancy frequency N and Coriolis parameter f). This radius can range from 30 to 300km in the atmosphere. The theoretical and numerical studies of [10] and of [12] showed that on the mesoscale with stable stratification, Coriolis effects lead to sharp gradients in the flow, generation of potential vorticity banners, and the formation of wind jets in elongated regions with transverse length scales of order L_R situated both upwind of the surface regions [14] and in ‘wake’ regions extending downwind (see also [7]).

The objective of this study is to model mesoscale flow in stable conditions when there are sharp changes in surface conditions on the scale of order of the inversion layer height h_o (i.e. 1-10km), i.e. to explain how the wind field is deflected, where wind jets appear, and how the boundary layer depth changes (which affects cloudiness and precipitation). Additionally, the study indicates the limitations of current operational mesoscale models, which, for example, fail to identify coastal wind jets or predict correctly how barrier jets interact with buoyancy driven flows on slopes. Conceptual and modelling improvements should help to improve the practically important predictions of currents, waves, and wind energy in coastal areas, and of urban pollution in confined valley flows. An equally important application of this study is to improve the representation or parameterization of mesoscale processes in numerical weather/climate prediction models, in which there is considerable uncertainty.

We consider steady flows and assume that the mean velocity and temperature (or density $\bar{\rho}$) are well mixed (i.e. near neutral conditions) in the lower troposphere. But above this level the atmosphere is stably stratified, i.e. a low level inversion. In order to predict how the flow in the boundary layer and the lower levels of the troposphere respond to the changing surface conditions we develop a simple linearised, steady-state perturbation model consisting of two layers of fluid (or flow) separated by a density jump ($-\Delta\rho$). The upper layer is approximated as a thin stable layer with uniform velocity U_o . The lower layer represents the shallow boundary layer (also referred to as the inversion layer). The general equations of this ‘shallow layer’ model are derived in section 2. In section 3 the model equations are used to show how flow adjusts to sharp changes in surface conditions. In section 4 we compare shallow layer model results with numer-

ical mesoscale simulations and examine the effect of varying the grid size.

2 SHALLOW LAYER MODEL FOR IDEALISED MESOSCALE FLOWS IN STABLE LAYERS

Figure 1 illustrates the idealised forms of the vertical variation of the upwind density and velocity. Upwind conditions of the model are assumed to be steady and uniform. The two layers of this flow are separated at the inversion height h_o , with the upper layer defined as $z > h_o$ and the lower layer as $z < h_o$. The density gradient in the upper layer is stable. The wind speed $U(z)$ varies significantly in the surface layer, $z < h_s$, situated at the bottom of the lower layer. Over most of the lower layer and in the upper layer there is an approximately constant wind speed of U_o . The entire vertical variation of density is a step change $\rho_o\Delta\rho_o$ at the height h_o . Fig. 1 also illustrates the perturbations to the flow. In response to the changing surface elevation z_S and surface roughness length z_o , the boundary layer height l_S and inversion layer height h_o are shown increasing downwind. Modified velocity and density profiles are also shown.

The perturbations to the flow are caused by (i) variations in the surface roughness length from z_{oo} to z_o , leading to an internal shear layer of depth l_S over the adjustment length \mathcal{L}_S [1], (ii) change in surface elevation z_S over a distance D_S which causes both horizontal pressure gradients produced by buoyancy forces and by shear stresses and flow separation [10] [3], and (iii) surface heating or cooling (which leads to a change in the density by $\gamma\rho_o$ where γ is a coefficient which varies over the region).

For typical complex mountainous terrain (as shown in Fig. 1) extending over a mesoscale distance L , the average effects of surface drag elevation change and changed buoyancy forces on the perturbations in the lower layer are modelled by introducing effective along-wind F and crosswind G body forces acting on the flow over length scales of the order of the typical adjustment distance \mathcal{L}_S (as in [10]). The forces here are averaged over the depth of the inversion layer (i.e. $0 < \hat{z} < h^*$, where $\hat{z} = z - z_S(x, y)$) and are parameterised by coefficients C_F, C_G . In general the overall adjustment length within the lower layer, \mathcal{L} , extends upwind and downwind beyond the region of length L over which the surface conditions are changed.

To study the leading order perturbation the advective terms are determined by the mean velocity U_o . Because of turbulence and, in stable flows, the action of internal waves, the horizontal perturbation velocity components u, v are assumed here to be approximately constant with height. The flow field is governed by the linearised shallow water equations which are given as [8],

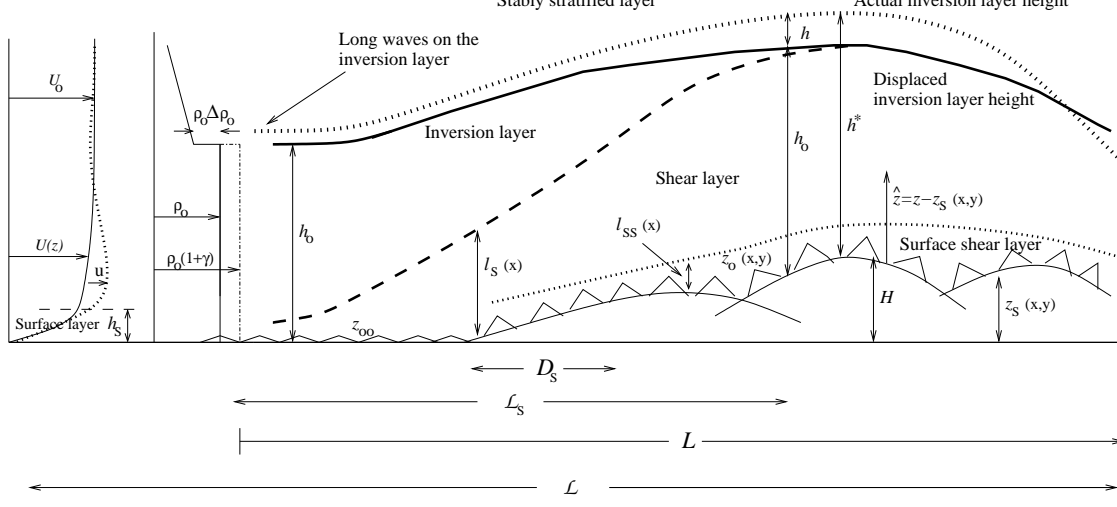


Figure 1: Simplified vertical profiles of velocity and density of a perturbed stable ‘shallow layer’ flow where the surface elevation z_S and roughness length z_o change over a distance L . Also the surface is cooled so that the density change $\gamma\rho_o$ is positive and varies with x . The changing surface conditions extends a horizontal distance (or width) B perpendicular to the flow (not shown). The thick dotted black line shows the changing inversion layer height h^* of the perturbed flow from its upwind value h_o . The dashed thick black line shows the changing shear layer thickness l_S . H and D_S are typical heights and half lengths of the surface elevation changes. L_S and L are the adjustment lengths for the horizontal shear layer and the overall mesoscale flow. h_s and l_{SS} are the depths of the upwind surface layer and the perturbed surface shear layer respectively. Note how the layer thickness is perturbed upwind.

$$Du = -\Delta g h_x + f v + \overline{F}, \quad (1a)$$

$$Dv = -\Delta g h_y - f u + \overline{G}, \quad (1b)$$

$$Dh = w(\hat{z} = h_o) = -[u_x + v_y] h_o, \quad (1c)$$

where w is the vertical velocity perturbation, h is the perturbation to the inversion height and $\Delta g = g\Delta\rho_o$ with g the acceleration due to gravity. Here $D = \partial/\partial t + U_o\partial/\partial x$. For the flow direction $\overline{F} = \overline{F}_D + \overline{F}_E + \overline{F}_H$, consisting of drag, elevation and heating components, with $\overline{F}_D = -C_F U_o^2/h_o$, $\overline{F}_E = -\Delta g \partial z_S/\partial x$ and $\overline{F}_H = h_o \Delta g \gamma_x$. Here C_F is a dimensionless coefficient for the surface drag which is much less than unity for surface roughness changes, where $C_F U_o^2/h_o = \Delta(-\overline{u'w'})_o/h_o$ (note the prime denotes turbulent fluctuations). Similarly in the crosswind or transverse direction, $\overline{G} = \overline{G}_D + \overline{G}_E + \overline{G}_H$, with $\overline{G}_D = -C_G U_o^2/h_o$, $\overline{G}_E = -\Delta g \partial z_S/\partial y$, $\overline{G}_H = h_o \Delta g \gamma_y$, and $C_G U_o^2/h_o = \Delta(-\overline{u'v'})_o/h_o$.

These equations lead to a general equation for h ,

$$D \left(\nabla_H^2 h - \frac{h}{L_R^2} - \frac{\mathbb{F}^2 D^2 h}{U_o^2} \right) = \mathbb{F} \frac{h_o}{U_o} \left[\frac{1}{L_R} [\overline{G}_x - \overline{F}_y] + \frac{\mathbb{F}}{U_o} D(\overline{F}_x + \overline{G}_y) \right] \equiv DR(x, y), \quad (2a)$$

where $\mathbb{F}^2 = U_o^2/(\Delta g h_o)$ and $R(x, y)$ is a ‘resistance/orography function’. On rescaling the horizontal scale in terms of the Rossby deformation radius L_R and the vertical deflections in terms of the layer thickness h_o , i.e. $\hat{h} = h/h_o$ and $(X, Y) = (x, y)/L_R$, for steady conditions ($\partial/\partial t = 0$), (2a) reduces to

$$\begin{aligned} \hat{\nabla}_H^2 \hat{h} - \mathbb{F}^2 \hat{h}_{XX} - \hat{h} &= \int_{-\infty}^X (\hat{G}_X - \hat{F}_Y)(X'') dX'' \\ + \mathbb{F}[\hat{F}_X + \hat{G}_Y] &\equiv \hat{R}(X, Y), \end{aligned} \quad (2b)$$

where $(\hat{F}, \hat{G}) = (L_R \mathbb{F}/U_o)(\overline{F}, \overline{G})$ and $\hat{R} = (L_R^2/h_o)R$. Here X'' is a variable of integration.

For low Froude number conditions the second term on the l.h.s of (2b) can be neglected. Combining typical thermal forcing (i.e. $\gamma \neq 0$) with low Froude number flow gives $F = \gamma_x \Delta g h_o$ and $G = \gamma_y \Delta g h_o$, so that $G_x - F_y = 0$, i.e. the integral in (2b) is zero. This considerably reduces the magnitude of the perturbations driven by thermal effects compared to those caused by roughness change.

From (1), equations for the normalised perturbations of the horizontal velocity \hat{u}, \hat{v} become:

$$\hat{u}_{XX} - \mathbb{F}^{-1}\hat{u}_Y = \mathbb{F}^{-2}[\hat{h}_{YY} - \mathbb{F}^2\hat{h}_{XX}] - \mathbb{F}^{-1}\hat{G}_Y \quad (2c)$$

$$\hat{v}_Y - \mathbb{F}^{-1}\hat{v} = -[\mathbb{F}^{-2} + 1]\hat{h}_X + \mathbb{F}^{-1}\hat{F}_X, \quad (2d)$$

where $(\hat{u}, \hat{v}) = (u, v)/U_o$.

3 GENERAL INTERPRETATION OF MODEL EQUATIONS

Here we use equation (2b) to show broadly how the flow adjusts with and without the Coriolis effect.

3.1 Upwind effects

Figure 2(a) shows a narrow strip of rough elevated terrain placed perpendicular to the flow with length $2D_S$ and a large transverse width $2B$. Suppose the perturbed surface conditions are caused by increased roughness and drag (so that $C_F > 0$ and $\partial z_S/\partial x = 0$) extending in the flow direction downwind from $x = 0$, and suppose that they extend a long way in the y direction (i.e. $B \gg L$ so that $\partial/\partial y = 0$). Then, (2a) shows that at low Froude number and with no Coriolis effect ($f = 0$),

$$\frac{\partial^2 h}{\partial x^2} = R(x) = \frac{\mathbb{F}^2 h_o \bar{F}_x}{U_o^2}, \quad (3a)$$

where $R \neq 0$ for $x > 0$. Let $\bar{F}(x)$ be a step function with maximum value $\Delta\bar{F}$, i.e. $\bar{F} = \Delta\bar{F}\mathcal{H}(x)$ where $\mathcal{H}(x)$ is the unit Heaviside function. Then $\bar{F}_x(x) = \Delta\bar{F}\delta(x)$ where $\delta(x)$ is the Dirac delta function, so that h and u are only perturbed for $x > 0$. From equations (2c) they are related by

$$u = -\frac{U_o h(x)}{h_o} \propto x\mathcal{H}(x). \quad (3b)$$

If the surface elevation increases by z_S , the solution to (3a) shows that h decreases by z_S .

However when Coriolis effects are present ($f \neq 0$) they affect the flows on length scales of the order L_R and the form of (2a) changes to

$$\frac{\partial^2 h}{\partial x^2} - \frac{h}{L_R^2} = R(x) = \frac{\mathbb{F}^2}{U_o^2} h_o \bar{F}_x, \quad (3c)$$

where $R(x) \neq 0$ for $x > 0$. (To first order $\bar{G} = 0$; see [11])

This equation means that even though $h \rightarrow 0$ as $x \rightarrow -\infty$, the effects of $R(x)$ extend upwind a distance of order L_R . (By contrast, for a continuously

stratified flow the disturbance may extend upwind a greater distance which is of the order of the width of the perturbed surface region B if $B > L_R$; see [10].)

The governing equation for the velocity field derived from (2c) and (2d) in terms of h now includes the Coriolis effect, so that u is still given by (3b), but v is given to lowest order by

$$v = U_o \mathbb{F}^{-1} h_x, \quad (3d)$$

which shows how the flow turns in a direction parallel to the contours of increased roughness and elevation [14], i.e. a barrier jet.

3.2 Transverse and downwind effects

If the surface region extends in a direction parallel to the wind (as in Fig. 2(a)), and F and G vary sharply in the y direction, then (2a) reduces to

$$\frac{\partial^2 h}{\partial y^2} - \frac{h}{L_R^2} = R(y) = \frac{\mathbb{F}h_o}{U_o^2 L_R} \int_{-\infty}^x -\bar{F}_y(x'') dx'', \quad (3e)$$

where $R(y) \neq 0$ for $y > 0$. (Here $\bar{G} = 0$.)

This shows that the flow perturbation in the transverse y direction also extends over a distance L_R when Coriolis effects are significant. Along these ‘edges’ separating the change in surface roughness or elevation, the forcing functions may be significant because $\partial F/\partial y$ is large. For sharp roughness change in the y direction, if the edge-line is exactly parallel to the wind, the integral portion of (3e) increases steadily downwind so that $R \propto x\delta(y)$ until non-linear effects become significant. But for a sharp elevation change in the y direction, i.e. $R \propto \delta(y)$, there is no variation in h or u downwind.

The velocity perturbation u is given (when $f \neq 0$) by (1b), so that (if $G = 0$),

$$u = \frac{-\Delta g h_y}{f}. \quad (3f)$$

Note how the two terms \bar{F}_x and $\int -\bar{F}_y(x'') dx''$ (in (3c) and (3e) respectively) produce a large anti-symmetric forcing and a smaller (by a factor \mathbb{F}) symmetric forcing of the inversion height. This in turn produces a large symmetric, and a smaller antisymmetric, streamwise velocity perturbation u , both of which extend further with Coriolis effects. Note that the larger antisymmetric effect on h only exists if Coriolis forces are present. If not, there is only the symmetric local perturbation. These effects can also be explained in terms of the perturbations of potential vorticity generated by the vertical deflection of the streamlines and by the resistance of the terrain (see [10]).

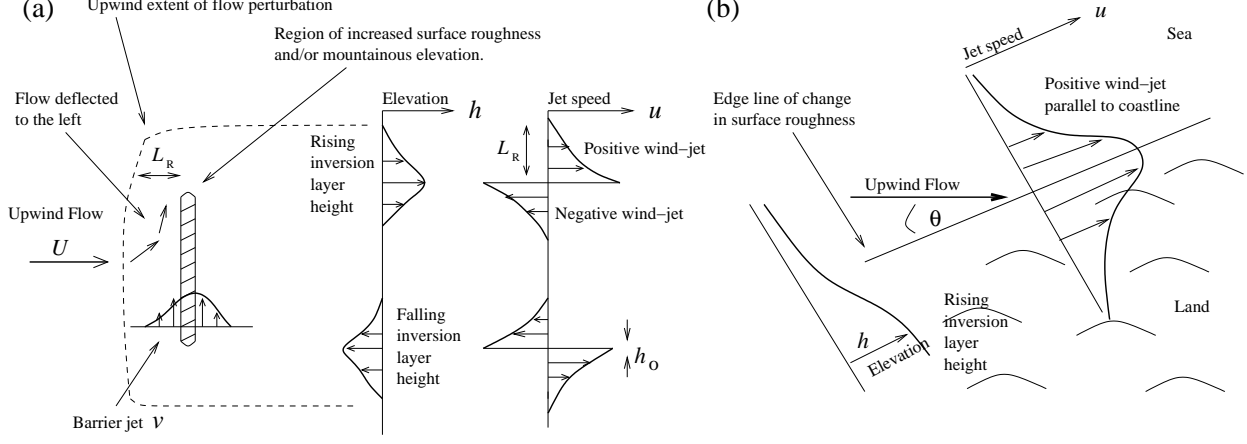


Figure 2: Diagram shows flow (a) parallel to, and (b) at an angle θ to, a sharp change in surface roughness or elevation. In (a) positive and negative wind jets are shown either side of the edge-line, and the height of the inversion layer is shown to rise/fall on the left/right hand side of the flow. The flow direction is deflected to the left, and the well known barrier jet is parallel to the incident surface. The wind jets are shown extending over a distance L_R , with rapid variation occurring on a scale h_o . In (b) a coastal wind jet is shown parallel to the coast, with the inversion layer height increasing over land.

3.3 Flow perturbations for a finite area of resistance

If the area of resistance extends over finite distances D_S and B in the flow and transverse directions respectively, the governing equation becomes two dimensional, so that

$$\nabla_H^2 h - \frac{h}{L_R^2} = R(x, y), \quad (4)$$

where $R \rightarrow 0$ when $|y| \geq B$ and $x/D_S \leq -1$.

But for $x \rightarrow \infty$, R is defined by an integral of the resistive force in the streamline direction, i.e. $R \rightarrow R_\infty(y) = f/(\Delta g U_o) \int_{-\infty}^{\infty} -F_y(x'', y) dx''$. If F is symmetric, this leads to the asymmetric displacements of the isopycnals on the ‘left’ and ‘right’ of the centre line of the disturbance region for both resistance and elevation changes. In the former case these extend downwind from the area of resistance [10], but not in the latter case of elevation change only (e.g. [2]). Note that near the region of resistance where $F_x \neq 0$, if the resistance and elevation are symmetrical about $y = 0$, the first order displacements are also symmetrical. The perturbations h, u , and v extend only over a distance of order L_R upwind of the region of resistance, unlike the flow with uniform stratification when the perturbations extend over a distance B (if $B > L_R$) (see [10]).

3.4 Roughness boundaries at arbitrary angles to the wind direction

Usually, at boundaries between smooth and rough terrain, the wind is neither parallel nor perpendicular, but rather lies at some angle θ from the edge. As shown by Fig. 2(b). If $\alpha = 1/\tan\theta$, to the leading order, the normalised drag force term is,

$$\hat{F}_D = -\hat{C}_F \mathcal{H}(X - \alpha Y). \quad (5)$$

Therefore the forcing functions on the r.h.s of (2b) can be expressed in terms of the normal coordinate \hat{n} ($= n/L_R$) and the resistance function $\hat{R} = \hat{R}^{(0)} + \mathbb{F}\hat{R}^{(1)}$, where

$$\hat{R}^{(0)} = -\hat{C}_F \propto \mathcal{H}(\hat{n}) \quad (6a)$$

$$\hat{R}^{(1)} = -\hat{C}_F \delta(\hat{n}). \quad (6b)$$

The solutions to (2b) can be expressed conveniently in terms of local functions $J^{(0)}(\hat{n})$ and $J^{(1)}(\hat{n})$, as

$$\hat{h}^{(0)} = \frac{\hat{C}_F J^{(0)}(\hat{n})}{\tan\theta} \quad (7a)$$

$$\hat{h}^{(1)} = \frac{\hat{C}_F J^{(1)}(\hat{n})}{\tan\theta}, \quad (7b)$$

where $J^{(0)} = 1/2 [e^{\hat{n}} \mathcal{H}(-\hat{n}) + (2 - e^{-\hat{n}}) \mathcal{H}(\hat{n})]$ and $J^{(1)} = 1/2 e^{-|\hat{n}|}$.

Thus the inversion layer depth increases ‘inland’ over the scale L_R , but the transition is not monotonic because the first order term contributes a local peak (see Fig. 2(b)).

Thence to leading order

$$\hat{v} = -\cos\theta \hat{C}_F [J^{(0)}(\hat{n}) + \mathbb{F}J^{(1)}(\hat{n})], \quad (8)$$

and

$$\hat{u} = \frac{\mathbb{F}^{-1} \hat{C}_F \cos\theta}{\sin\theta} [J^{(0)' }(\hat{n}) + \mathbb{F}J^{(1)' }(\hat{n})] + 0(\mathbb{F}), \quad (9)$$

where $J^{(0)'}(\hat{n}) = 1/2 e^{-|\hat{n}|}$ and $J^{(1)'}(\hat{n}) = -1/2 e^{-|\hat{n}|} \text{sgn}(\hat{n})$.

Thus the transverse component of velocity \hat{v} decreases to zero outside the roughness strip on a scale L_R (not shown), while the parallel component \hat{u} develops a jet centred on the edge-line separating the change in surface conditions (see Fig. 2(b)).

A further implication of this non-linear correction occurs if the coast or roughness boundary curves in such a way that, to first order, the wind remains parallel to the coast. Then the wind speed continues to increase with distance along the coast, i.e. to the left of the prevailing wind in the Northern hemisphere.

4 COMPARISON BETWEEN SHALLOW LAYER MODEL AND NUMERICAL MESOSCALE RESULTS

In this section, the quantitative estimates and general concepts of mesoscale flows detailed in sections 2 and 3 are compared to numerical mesoscale simulations of flows over mountainous and surface roughness change computed using the non-linear Met Office ‘Unified Model’. The computed flows are over southern Greenland using UM 4.5 at a horizontal resolution of approximately 12km and the Dover-Straits region of the English Channel using UM 5.1 at horizontal resolutions of approximately 12 and 2km.

4.1 Numerical model description

The UM is a Numerical Weather Prediction (NWP) model which can be run as a mesoscale model. [4] provides a detailed description of the hydrostatic model UM 4.5 and [5] of the non-hydrostatic model UM 5.1 (also called the ‘New Dynamics’). Both versions use a nested limited-area domain. Lateral boundary conditions are generated by nesting the limited-area domain within the global model [4]. For the Greenland flow simulation a 182 by 146 latitude-longitude grid with 0.11° ($\sim 12\text{km}$) resolution and 38 model levels in the vertical was centred over southern Greenland. Two nested domains were required for the Dover Straits simulation, the ‘outer’ a 182 by 146 latitude-longitude grid with 0.11° ($\sim 12\text{km}$) resolution centred over the UK and the ‘inner’ a 280 by 340 latitude-longitude grid with 0.02° ($\sim 2\text{km}$) resolution centred over southeast England, both with 38 model levels in the vertical.

4.2 Comparison with numerical mesoscale simulation over a mountain flow at 12km resolution

The topography of Greenland is characterized by large and very steep elevation change between the coastal margins and the central plateau ($\sim 3000\text{m}$) and rough [$z_0 \sim 1 - 10\text{m}$], mountainous terrain around the coasts. The specific case considered occurred on 9 November 2000. Fig. 3 presents the 1800 UTC simu-

lation of 10m-wind computed using UM 4.5 at 12km horizontal resolution. We concentrate on flow modification due to the western coast of Greenland and comparison of the mesoscale simulation with the above shallow layer model features.

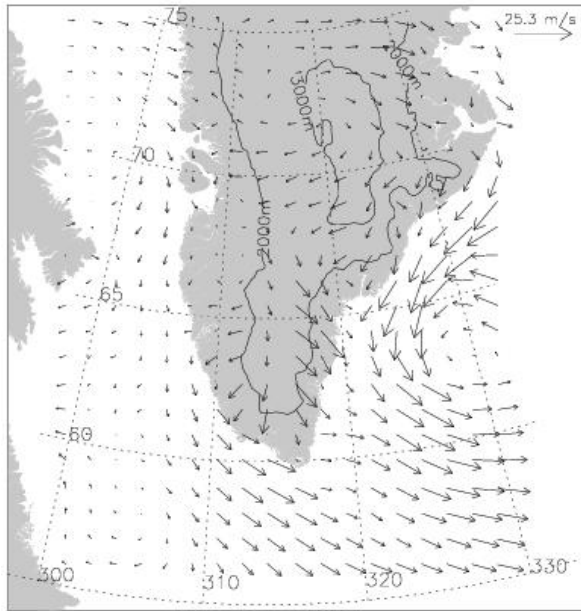


Figure 3: Atmospheric westerly flow over southern Greenland computed using UM 4.5 with a horizontal resolution of 12km. Orography elevation contours are 2000m and 3000m. Shown are 10m-wind speed (ms^{-1}) vectors (every 8 grid points).

Figure 3 shows the upstream region characterized by a well defined, though relatively weak, low-level westerly flow ($< 4\text{ms}^{-1}$) which is blocked by the low Froude number flow (for $U = 4\text{ms}^{-1}$, a typical value of stability as $N \sim 0.01\text{s}^{-1}$ and $H \sim 3000\text{m}$, $\mathbb{F}_H = U/NH = 0.13$), forcing the flow south at 10m-wind speed $\sim 5\text{ms}^{-1}$. The flow develops into a well defined wind jet travelling parallel to the coastline, with wind speeds of about 8ms^{-1} , increasing markedly to above 15ms^{-1} as it nears the southern tip. On the slopes of the land mass, katabatic winds develop with a wind speed of about 4ms^{-1} which flow in to the wind jet. The air flow separates at the southern tip of Greenland where there is a sharp change in the direction of the coastline due to a combination of baroclinic effects at the edge of the plateau and boundary layer effects in the lower level horizontal flow [9]. The wind jet continues as a westerly flow downwind of the tip in the wake, its velocity decreasing gradually (down to 10ms^{-1} over 1000km) [7].

For this flow the Rossby deformation radius (based on mountain height H) $L_R^H = NH/f \sim 230\text{km}$ (for $f \sim 1.3 \times 10^{-4}\text{s}^{-1}$). Inspection of contoured data shows sharp gradients of velocity parallel to the entire coastline with the highest velocities and wind jet

centred close to the coastline decreasing over a transverse length scale of order 150-200km, i.e. of order of L_R^H . These features are consistent with shallow layer flow (see Fig 2(a)) over a rough elevated strip that is very wide compared to L_R , as well as with the continuously stratified calculations of [7].

4.3 Comparison with numerical mesoscale simulation of flow with change in surface roughness at 12 and 2km resolution

Here we investigate numerical mesoscale modelling of flow over a sudden change in surface boundary condition at two horizontal resolutions, 12 and 2km (i.e. of order h_o). The case considered is a northeasterly flow over the land of the Kent Peninsula and down the Dover Straits region of the English Channel on 23 July 2000, where a significantly increased wind speed was observed by comparison with that over the North Sea. The Dover Straits are around 30km wide at their narrowest dimension and over 300km in length and lie in a gap in the orographic barrier which is 150-200m in height. These flow conditions correspond approximately to flow modelled by a change in roughness boundary at arbitrary angle to the wind direction (section 3.4) as the air moves from sea to land (i.e. $\mathbb{F}_H \gg 1$ so air passes over the orography, and is only weakly channelled around it).

Figures 4 and 5 present the 1300 UTC simulation of 10m-wind computed using UM 5.1 at horizontal resolutions of 12 and 2km. Both simulations show a positive low-level jet starting at the entrance to the Dover Straits and extending westwards over about 150 kilometers. Comparing the two figures, the higher resolution data shows the position of the wind jet running further north, following much more closely the contours of the English coastline, and with sharper gradients in velocity normal to the coastline. These features correspond to the shallow layer model predictions of section 3. Though both runs show wind speeds in excess of 12ms^{-1} , the peak wind speed is higher at 2km resolution, as is the extent of the speed-up area. Additionally, the higher resolution data shows a marked strengthening of the wind along the r.h.s of the English coastline (looking downwind) which is not apparent at coarser resolution.

For the observed values of $\Delta\rho/\rho$ and h_o [3], with $f \sim 1.2 \times 10^{-4} \text{s}^{-1}$, the Rossby deformation radius is $L_R = Nh_o/f \sim 100\text{km}$. Figs. 4 and 5 show a significant perturbation (of about 25%) of the surface wind speeds upwind of the Kent coast, extending over a distance of about 20-30km at higher resolution, and a some what greater extent of 50-70km at the coarser resolution (perhaps because of the coarser representation of the width of the Kent Peninsula). But both these results are broadly consistent with the shallow layer model. The higher resolution results show how

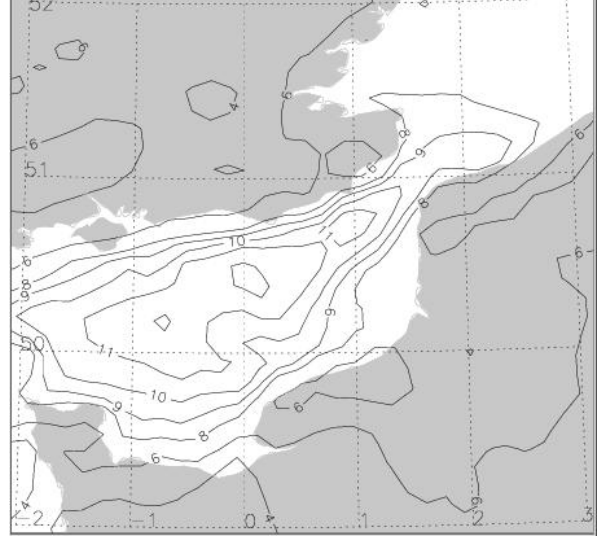


Figure 4: 10m-wind speed (ms^{-1}) with contour interval 1ms^{-1} over the Dover Straits, computed using UM 5.1(1) with a horizontal resolution of 12km.

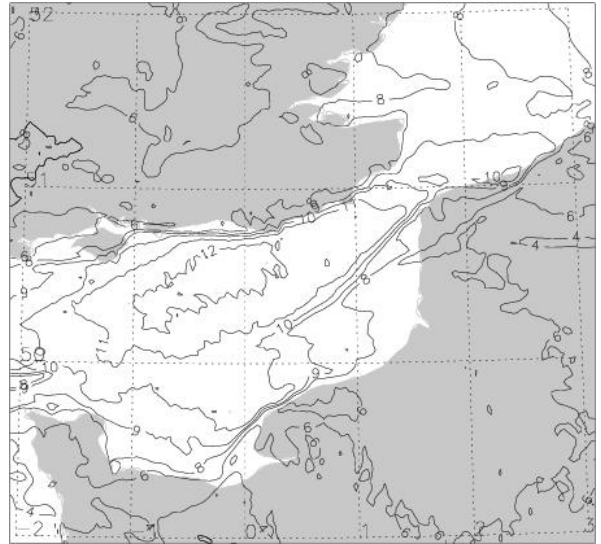


Figure 5: 10m-wind speed (ms^{-1}) with contour interval 1ms^{-1} over the Dover Straits, computed using UM 5.1(2) with a horizontal resolution of 2km.

there are very sharp increases of wind speed within 1-2km of the coast which increase in the downwind direction and decrease away from the coast over about 20km. The coarser resolution doesn't model this effect so clearly and the maximum wind speed is of order 10-15km from the coast, i.e. comparable with the grid size and an order of magnitude greater than h_o .

5 CONCLUSIONS

This paper provides an overview of the effects on mesoscale flows of variations of surface roughness and elevation when the approach flow has a stable inversion layer. Under these conditions, systematic errors in mesoscale predictions may have been overlooked in the past because there has been some con-

ceptual uncertainty about the upwind and lateral effects. The idealised modelling suggests that the flow response to changing surface conditions causes sharp gradients in the flow, i.e. the formation of positive and negative jets. When the approach flow is parallel to, or at an angle to, a edge-line separating extending regions of low and high surface roughness, e.g. a coastline, a cape, or a ridge of hills, the theory shows how the perturbation wind speed u increases with distance until a non-linear mechanism comes into play. The jets are most pronounced in elongated regions with transverse length scales of the order of the Rossby Deformation radius L_R , reaching their maximum value within a distance from the edge-line of the order of h_o , which may be as low as 1km. In particular, the flow response to changing surface conditions has both similarities and differences when there are elevation changes and drag effects due to surface roughness changes. For example, both have upwind effects but only drag causes significant increases in the wind speed perturbation in the downwind flow direction or parallel to roughness change. Other related rapidly changing meteorological variables are deflection of the wind field and boundary layer depth. For example, inversion height h_o and cloudiness increase inland from the coast as stable airflow approaches from the sea. The results demonstrate the importance of fine scale modelling. At horizontal resolutions of order h_o or less (i.e. 2km), numerical mesoscale results are consistent with very fine scale features of the shallow water flow. However, even at a larger resolution of 12km, certain broad features (e.g. parallel wind-jets) are well captured. The length scales imply that any operational models currently used or planned for the next few years will fail to describe these features unless the grid size is at least as small as this dimension. Future development might involve establishing limits of current models and producing subgrid scale parameterisation schemes or models near these critical regions, as is usual for other processes.

This work was supported by grants from NERC to CPOM, Dept. of Space & Climate Physics and to Mathematics at UCL. Thanks to Rachel Capon for supplying the Dover Straits numerical simulations.

REFERENCES

- [1] Belcher, S. E., Xu, D. P. and Hunt, J. C. R., ‘The response of the turbulent boundary layer to arbitrarily distributed surface roughness changes’, *Q. J. R. Meteorol. Soc.*, **116**, 611–635, 1990.
- [2] Buzzi, A. and Tibaldi, S., ‘Inertial and frictional effects on rotating and stratified flow over topography’, *Q. J. R. Meteorol. Soc.*, **103**, 135–150, 1977.
- [3] Capon, R., ‘Modelling low level winds with the Met Office New Dynamics model’. Internal report No. 133, NWP Scientific Paper No. 66, Met Office, JCMM, Reading University, Reading, UK, 2002.
- [4] Cullen, M. J. P., ‘The unified forecast/climate model’, *The Meteorological Magazine*, **122**, 81–94, 1993.
- [5] Cullen, M. J. P., Davies, T., Mawson, M. H., James, J. A., Coulter, S. C. and Malcolm, A., ‘An overview of numerical methods for the next generation UK NWP and climate model’. Canadian Meteorological and Oceanographic Society, Numerical methods in atmospheric and oceanic modelling. The Andre J. Robert memorial symposium held in Montreal, Canada, October 5-7, 425–444, 1997.
- [6] Doyle, J. D., ‘The influence of mesoscale orography on a coastal jet and rainband’, *Mon. Weather Rev.*, **125**, 1465–1488, 1997.
- [7] Doyle, J. D. and Shapiro, M. A., ‘Flow response to large scale topography: the Greenland tip jet’, *Tellus*, **51A**, 728–748, 1999.
- [8] Gill, A. E., *Atmosphere-Ocean dynamics*. Academic Press, London, UK, 1982.
- [9] Hunt, J. C. R., Feng, Y., Linden, P. F., Greenslade, M. D. and Mobbs, S. D., ‘Low-Froude-number stable flows past mountains’, *Il Nuovo Cimento*, **20C**, 261–272, 1997.
- [10] Hunt, J. C. R., Olafsson, H. and Bougeault, P., ‘Coriolis effects on orographic and mesoscale flows’, *Q. J. R. Meteorol. Soc.*, **127**, 601–633, 2001.
- [11] Newley, T. M. J., Pearson, H. J. and Hunt, J. C. R., ‘Stably stratified rotating flow through a group of obstacles’, *Geophys. Astrophys. Fluid Dyn.*, **58**, 147–171, 1991.
- [12] Olafsson, H. and Bougeault, P., ‘The effect of rotation and surface friction on orographic drag’, *J. Atmos. Sci.*, **54**, 193–210, 1997.
- [13] Scorer, R. S., ‘Sunny Greenland’, *Q. J. Roy. Meteorol. Soc.*, **114**, 3–29, 1988.
- [14] Shutts, G., ‘Idealised models of the pressure force on mesoscale mountain ridges’, *Contrib. Atmos. Phys.*, **71**, 303–313, 1998.
- [15] Smith, R. B., ‘The influence of earth’s rotation on mountain wave drag’, *J. Atmos. Sci.*, **36**, 177–180, 1979.